

Segmentation of Abdominal Aortic Aneurysms in CT Images using a Radial Model Approach

Iván Macía¹, Jon Haitz Legarreta¹, Céline Paloc¹, Manuel Graña², Josu Maiora³,
Guillermo García⁴, and Mariano de Blas⁵,

¹ Biomedical Applications Department, VICOMTech, Donostia-San Sebastián, Spain
{imacia, jhlegarreta, cpaloc}@vicomtech.org

² Computational Intelligence Group, Computer Science Faculty, University of the Basque
Country, Donostia-San Sebastián, Spain
manuel.grana@ehu.es

³ Electronics and Telecommunications Department, ⁴ Engineering Systems and Automatic
Department, Technical University School, University of the Basque Country, Donostia-San
Sebastián, Spain
{j.maiora, g.garcia}@ehu.es

⁵ Interventional Radiology Service, Donostia Hospital, Donostia-San Sebastián, Spain
mariano.deblasbravo@osakidetza.net

Abstract. Abdominal Aortic Aneurysm (AAA) is a dangerous condition where the weakening of the aortic wall leads to its deformation and the generation of a thrombus. To prevent a possible rupture of the aortic wall, AAAs can be treated non-invasively by means of the Endovascular Aneurysm Repair Technique (EVAR), which consists of placing a stent-graft inside the aorta in order to exclude the bulge from the blood circulation and usually results in its contraction. Nevertheless, the bulge may continue to grow without any apparent leak. In order to effectively assess the changes experienced after surgery, it is necessary to segment the aneurysm, which is a very time-consuming task. Here we describe the initial results of a novel model-based approach for the semi-automatic segmentation of both the lumen and the thrombus of AAAs, using radial functions constrained by *a priori* knowledge and spatial coherency.

Keywords: abdominal aortic aneurysm, endovascular aneurysm repair, segmentation, region growing, image moments, radial functions.

1 Introduction

Abdominal Aortic Aneurysm (AAA) is a cardiovascular disease that is caused by a degenerative process of the aortic wall, which leads to its wear and deformation. If not treated, AAAs increase in size progressively and may result in rupture, and, eventually, death [1].

There are currently two main repair techniques for AAA: Open Aneurysm Repair (OR), and Endovascular Aneurysm Repair (EVAR). EVAR is a minimally invasive

technique where an endograft, typically a cloth graft with a stent exoskeleton, is placed within the lumen of the AAA, extending distally into the iliac arteries. This serves as a bypass and decreases the pressure on the aortic wall, leading to a reduction in AAA size over time and a decrease in the risk of aortic rupture. An Intraluminal Thrombus (ILT) forms in the majority of abdominal aortic aneurysms. Correctly excluded aneurysms progressively shrink after EVAR surgery. Nevertheless, there may be leaks into or from the sac due to incorrect positioning, displacement or torsion of the graft. In order to ensure that the graft is accomplishing its intended goal, close follow-up is required after endovascular repair, with CT scans performed at one, six, and 12 months, and then yearly.

In order to assess the evolution of the bulge, the aneurysm must be delineated. Due to low-contrast in the ILT region compared to adjacent structures, the segmentation of the thrombus is not a trivial task. Manual segmentation by trained radiologists is a time-consuming task, and suffers from intra- and inter-observer variability.

Thrombus segmentation of AAAs has been addressed less frequently in the literature [2][3][4][5][6]. The works presented in [2] and [3] need initial manual delineations to initialize their models, and the method by de Bruijne *et al.* [3] needs posterior user intervention in case of thrombus boundary overflow. Olabarriaga *et al.* [4] employ a binary thresholding to obtain the lumen, which is used as an initialization for a deformable model to segment the thrombus. Simple thresholding takes into account other tissues not connected to the lumen, so further processing is usually needed to avoid those structures. Furthermore, the use of deformable models needs a fine parameter optimization to obtain acceptable results. Zhuge *et al.* [5] present an algorithm based on a level-set approach whose main advantage is the automatization and parameter insensitivity. Nevertheless, the required time (order of several minutes) is a main drawback. The works by Borghi *et al.* [6] make use of region growing segmentation techniques in order to obtain the lumen boundary, but then use manual delineation of the aneurysm wall to obtain a 3D model of a TAA (Thoracic Aortic Aneurysm).

In this paper, we present the preliminary results of a novel semi-automatic 3D technique for the segmentation of the AAA lumen and thrombus. Segmentation of the lumen is based on a 3D region growing algorithm starting from two or more manually selected seed points. The aortic centerline is calculated from the lumen segmentation using an image moment on connected components. The thrombus contour is modeled as a radial function. Starting from the centerline, a polar resampling of the input image is obtained. This image is analyzed by obtaining radial and slice-level connected components which are filtered based on *a priori* knowledge and spatial coherency. The radial function for the thrombus is obtained from the resulting connected components and defines the target segmented region. The main advantages of this method are its robustness and speed.

The remainder of this paper is organized as follows. The region growing algorithm for lumen segmentation is explained in Section 2. The proposed centerline extraction technique is explained in Section 3. Thrombus segmentation is discussed in Section 4. Results and discussion are presented in Section 5 and finally, conclusions are provided in Section 6.

2 Region Growing based Lumen Segmentation

Segmentation of the lumen is based on a 3D region-growing algorithm. First, the image is preprocessed to reduce noise and a Volume of Interest (VOI) is defined in order to reduce the extent of the data. A seed point on the lumen is at least required for the region growing algorithm. The algorithm, implemented in ITK [7], includes voxels that lie in a confidence interval of the current segmented region over an iterative process. At each iteration, all neighborhood voxels are visited and the confidence criterion is evaluated. Then, statistics are recomputed and the next iteration begins.

The resulting segmentation is smoothed by morphological closing, which also fills possible small holes.

3 Centerline Extraction

The centerline approximates the centroid of the lumen region at each slice and is a good approximation of the morphological skeleton of the whole aorta. It also serves as the starting point for the thrombus segmentation. A single point on the centerline is obtained for every slice, since the aorta is almost normal to axial slices.

The centerline extraction is performed on a slice-by-slice basis using 2D image moments. Image moments provide information on the geometry features of a given structure. The moments of a 2D image are defined as

$$M_{p,q} = \sum_{y=0}^{Y-1} \sum_{x=0}^{X-1} x^p y^q I(x,y). \quad (1)$$

where $I(x,y)$ is a discrete image.

The centroid is defined as the pair $\left[\frac{M_{10}}{M_{00}}, \frac{M_{01}}{M_{00}} \right]$.

On each slice connected components are detected and the centroid of each object is computed. The Euclidean distance is then calculated from each of the candidate centroids to the centroid kept in the previous slice and the nearest candidate centroid is kept as the one corresponding to the structure of interest. The algorithm, described below, yields a series of points that when displayed in three dimensions depict the central line or skeleton of the lumen.

Algorithm 1. Centerline extraction.

- 1: Initialization of region: center line in first processed slice
- 2: Iterative process: **for** all slices in 3D image **do**
- 3: identify connected components
- 4: **for** components in slice **do**
- 5: compute candidate centroids
- 6: compute Euclidean distances to centroid in previous slice
- 7: **end for**

8: keep nearest candidate centroid
9: **end for**

4 Thrombus Segmentation

In this paper, we propose modeling the internal and external radius of the thrombus of the aneurysm as radial functions in cylindrical coordinates. Then, we can express the volume of interest around the lumen centerline as

$$\Psi = \Psi(r, \theta, z). \quad (2)$$

At every z value, we choose the origin of these functions to be the centerline point at the corresponding slices. The external and internal radii of the thrombus and the aneurysm can be defined as two contours given by

$$\begin{aligned} T_{\text{rint}} &= \Psi_{\text{rint}}(\theta, z) . \\ T_{\text{rext}} &= \Psi_{\text{rext}}(\theta, z) . \end{aligned} \quad (3)$$

The segmentation procedure consists of calculating the internal and external radii that define T_{rmin} and T_{rmax} at every point, and which enclose the region corresponding to the thrombus. The model is depicted in Figure 1.

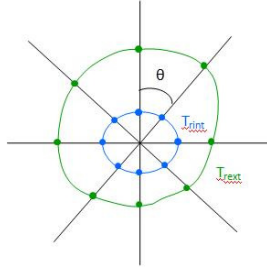


Figure 1. Radial model for the thrombus.

Conversion of Cartesian to polar coordinates requires resampling the input volume of interest. For every slice, a new image is obtained, where the X coordinate represents the radius, starting from the centerline point at the left, and the Y coordinate represents the angle, starting from the top and covering 360 degrees. This is represented in Figure 2, where an original slice is shown (left), together with its corresponding polar representation (center).

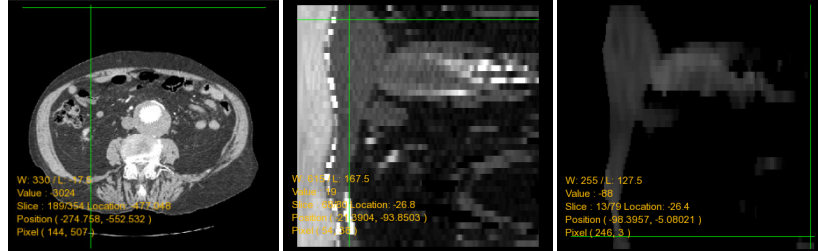


Figure 2. Axial slice (left), corresponding polar representation (center) and median filtered version with threshold for lumen and stent (right). Left origin is taken on the centerline on each slice for the polar representation.

The polar representation presents several advantages. First, the VOI is converted to a cylindrical VOI, instead of the typical rectangular prism, but it is treated as a standard volume with a regular grid. Second, the speed of the computations is increased, since resampling is only performed once and the polar slices are processed as standard images.

In order to remove noise, the polar image slices are filtered using a median filter. Each image is thresholded above 150 HU (Hounsfield Units) to a background value of -100 HU. This removes the lumen and the stent on the left side and makes the thrombus the brightest structure closest to the centerline. We can use this *a priori* information for the segmentation. The result is shown in Figure 2 (right), where significant noise has been eliminated and the structures of interest smoothed.

Localization of the external radius of the thrombus on each slice in polar coordinates is achieved by a local analysis based on two concepts: *radial connected components* (RCC) and *slice connected components* (SCC). We define an RCC as a connected component on a row of a polar slice and a SCC as a connected component on a polar slice. We store this RCCs using run-length encoding by just storing first and last index.

First, a row-by-row analysis is performed in all slices to create an image of RCCs. An RCC is created for consecutive pixels of a row that follow a given membership criterion. We use the absolute difference from the mean of the current RCC with a threshold value of 20 HU as the membership criterion. In the same process, the lumen radius is identified as the first RCC with an average value of -150 HU, as was set before by thresholding. The algorithm for creating the RCCs is as follows:

Algorithm 2. RCC extraction.

- 1: Initialization of region: center line in first processed slice
- 2: Iterative process: **for** all polar slices **do**
- 3: **for** all rows in current polar slice **do**
- 4: create new RCC and insert first voxel in row
- 5: **for** all voxels in current row **do**
- 6: **if** (intensity(voxel) \in Intensity range(RCC)) **then**
- 7: insert voxel in current RCC
- 8: **else**

```

9:             create new RCC and insert current voxel
10:          end if
11:        calculate and store lumen external radius for the row
12:      end for
13:    end for
14:  end for

```

Next, we proceed to filter the RCCs. First, RCCs whose average values are not in the range of 0-200 HU are removed. These values are quite conservative in order to be valid for most datasets. Second, RCCs that do not start 5 mm away from the external lumen radius are removed too. Results of the RCC computation procedure are shown in Figure 3. It can be seen that the thrombus has been almost completely isolated, but some RCCs that are not part of the thrombus still remain (Figure 3, right).

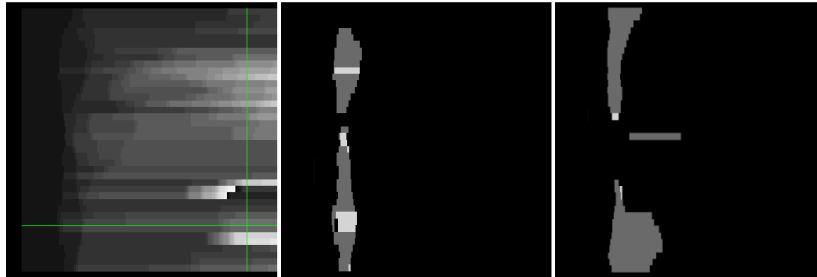


Figure 3. RCCs (left) and filtered RCCs (center and right). RCCs along each row are depicted using a different grey value.

SCCs are computed in a similar way, by using connectivity and the same intensity criteria as for the RCCs. Each SCC keeps a list of contained RCCs. SCCs are used to filter RCCs by using spatial coherency information on each slice. First, SCCs (and corresponding RCCs) that contain less than 10 voxels are discarded since they are not significant at a slice level. Next, SCCs are filtered by the position of the centroid. We compute the centroids of all the RCCs on a slice and calculate their median value. Then we compute the distance from the centroid of every SCC on that slice to the median centroid value and if the distance is greater than 20 mm the SCC is completely removed.

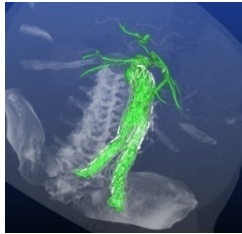
Initial values for T_{rint} and $T_{r_{ext}}$ are obtained by taking, for every row on all slices, the first index of the first RCC and the last index of the last RCC on that row. This results in a good approximation to the real external thrombus contour, with the exception of some areas where the thrombus region invades adjacent structures. These areas represent a discontinuity in the RCC as shown in Figure 5 (left).

In order to solve this problem, a continuity constraint is imposed over $T_{r_{ext}}$ where the contour points whose radii are part of a discontinuity are interpolated. Discontinuities are first identified as significant radius changes from line to line. Then, the radii in these areas are linearly interpolated in order to obtain the final result.

5 Results and Discussion

Our method has been initially tested on a real human contrast-enhanced dataset obtained from a LightSpeed16 CT scanner (GE Medical Systems, Fairfield, CT, USA) with 512x512x354 voxel resolution and 0.725x0.725x0.8 mm spatial resolution. Two points inside the lumen, defining the limits of the thrombus region in axial direction were manually selected as seed points for the segmentation of the lumen (Figure 4). The lumen centerline is then extracted from it and is used as the origin for the polar representation in an area of radius 10 mm around the centerline. Finally, the described radial function-based model is used to segment the thrombus.

Figure 4. Lumen segmentation.



Initial results of the thrombus segmentation method can be seen in Figure 5 where the initially estimated and the corrected external contours of the thrombus are shown. The thrombus segmentation shows promising results in defining the external contour, whose density is very similar to adjacent structures, and very prone to segmentation leaks in those areas. One of the main advantages of the method is its computational speed. It took less than 20 s to process 80 slices on a Pentium Core 2 Quad at 2.4 GHz. However, the method requires further improvements, since we have observed an underestimation of the radius in some places which were identified as leaks (Figure 5, right).

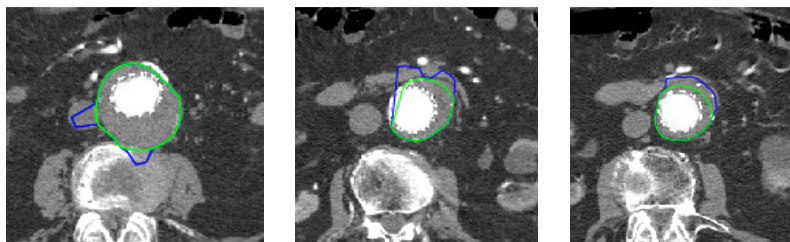


Figure 5. Correction (green) of the initial thrombus external radius (blue). Right correction (left and right) and underestimation (right).

6 Conclusion

We have developed a novel technique for (semi-)automatic segmentation of AAAs. The lumen is obtained applying a region-growing-based algorithm, from which the centerline is obtained for use as the origin of a polar coordinate representation of the input slices. The thrombus is modeled as a radial function that varies with the angle and the slice starting from the centerline. The function for the external radius is obtained by local and slice-level analysis of connected components and an *a priori* knowledge of the location, size and intensity of the thrombus.

The algorithm does not depend on any user-defined contour or initial manual segmentation. User interaction is minimal: it only needs two seed points contained in the lumen and defining the range of slices of interest. Moreover, the speed of the whole process makes it also suitable for routine clinical use.

The algorithm is being initially tested on human datasets and results are promising. Accurate segmentations are obtained in areas where it is difficult to distinguish the thrombus from adjacent structures.

Future work will be oriented to improve the thrombus model, fine-tune the parameters of the process for a large number of datasets and validate the segmentation by comparison with manual segmentations and other methods.

Acknowledgments. This work is sponsored and partially financed by the Basque Government through the INTEK Program. We also thank the companies Bilbomatica and eMedica for their participation in this work.

References

1. Upchurch, G.R., Jr., Schaub, T.A.: Abdominal Aortic Aneurysm. In Am Fam Physician. 73(7):1198-204 (Apr 2006)
2. Subasic, M., Loncaric, S., Sorantin, E.: 3D Image Analysis of Abdominal Aortic Aneurysm. In: Sonka, M., Fitzpatrick, M. (Eds.), Medical Imaging: Image Processing. Proceedings of SPIE, 4684: 1681–1689 (2002)
3. de Bruijne, M., van Ginneken, B., Viergever, M.A., Niessen, W.J.: Interactive Segmentation of Abdominal Aortic Aneurysms in CTA Images. Medical Image Analysis, 8(2): 127-38 (2004)
4. Olabariaga, S.D.; Rouet, J.-M., Fradkin, M., Breeuwer, M.; Niessen, W.J.: Segmentation of Thrombus in Abdominal Aortic Aneurysms from CTA with Nonparametric Statistical Grey Level Appearance modelling. IEEE Transactions on Medical Imaging, 24(4): 477- 485, IEEE Press, New York (2005)
5. Zhuge, F., Rubin, G.D., Sun, S., Napel, S.: An Abdominal Aortic Aneurysm Segmentation Method: Level-set with Region and Statistical Information. Med Phys, 33 (5):1440-1453 (May 2006)
6. Borghi, A., Wood, N.B., Mohiaddin, R. H., Xu, X.Y.: 3D Geometric Reconstruction of Thoracic Aortic Aneurysms. BioMedical Engineering OnLine, 5:59 (Nov 2006).Radiology and Surgery. Excerpta Medica International Congress Series, 1191: 213–217. Elsevier Publishers, Amsterdam (1999)
7. Ibanez, L., Schroeder, W., Ng, L., Cates, J.: The ITK Software Guide. Kitware Inc. (2003) ISBN: 1-930934-10-6